Chemical Science

ROYAL SOCIETY OF CHEMISTRY

EDGE ARTICLE

View Article Online
View Journal | View Issue

Cite this: *Chem. Sci.*, 2022, **13**, 7341

All publication charges for this article have been paid for by the Royal Society of Chemistry

Received 10th February 2022
Accepted 1st June 2022

DOI: 10.1039/d2sc00836j

rsc.li/chemical-science

Photostable polymorphic organic cages for targeted live cell imaging†

Dana Al Kelabi,‡[a] Avishek Dey,‡[a] Lukman O. Alimi,[a] Hubert Piwoński,[b] Satoshi Habuchi[b] and Niveen M. Khashab*[a]

Fluorescent microscopy is a powerful tool for studying the cellular dynamics of biological systems. Small-molecule organic fluorophores are the most commonly used for live cell imaging; however, they often suffer from low solubility, limited photostability and variable targetability. Herein, we demonstrate that a tautomeric organic cage, **OC1**, has high cell permeability, photostability and selectivity towards the mitochondria. We further performed a structure–activity study to investigate the role of the keto–enol tautomerization, which affords strong and consistent fluorescence in dilute solutions through supramolecular self-assembly. Significantly, **OC1** can passively diffuse through the cell membrane directly targeting the mitochondria without going through the endosomes or the lysosomes. We envisage that designing highly stable and biocompatible self-assembled fluorophores that can passively diffuse through the cell membrane while selectively targeting specific organelles will push the boundaries of fluorescent microscopy to visualize intricate cellular processes at the single molecule level in live samples.

Organic fluorophores are of great interest in many research fields especially live cell imaging, which allows for noninvasive observation and monitoring of biological processes. Small molecule fluorophores can be functionalized and tuned with high precision to tag a diverse variety of biological targets; however, limited water solubility, cell-permeability, photostability and targetability have halted the biomedical translation of many promising fluorescent molecules.[1] Ultimately, new generations of fluorescent tags were designed to include new functionalities that can improve their physical properties and cell penetration such as long aliphatic side chains and cell penetrating peptides.[2–6] In addition, various strategies have been employed to improve the photostability of these compounds by the addition of electron withdrawing groups, conformational changes, encapsulation or incorporation within host macrocycles.[7–13]

Major efforts in the organic fluorophores development have been directed towards designing stable probes targeting the mitochondria as it plays a central role in the generation of adenosine triphosphate (ATP), central metabolism, and apoptosis.[14,15] Successful examples of mitochondria targeting fluorophores include triphenyl phosphonium cations, heterocyclic aromatic cations, macrocyclic amphiphiles, BODIPY derivatives and mitochondria targeted peptides that have limited solubility.[16–21] Commercially available dyes for mitochondrial imaging such as Mito Tracker Red have a high photobleaching tendency and can form covalent bonds with the mitochondrial respiratory chain complex I resulting in increased cytotoxicity. Consequently, various organic, inorganic and hybrid platforms were developed ranging from small nanoparticles to self-assembled frameworks on the quest for improved mitochondrial imaging agents.[22–27]

Porous organic cages have received major attention over the last decade as they are easily prepared, soluble in a range of solvents and are intrinsically porous.[28–31] They have shown excellent applicability in molecular recognition, sensing and hydrocarbon separation but their biomedical imaging applications have never been investigated.[32–35] Recently, self-assembled organic imine stacks showed impressive electroluminescence and live cell imaging.[36] Moreover, an intracellular targeted macrocyclic nanohoop showed fast cell uptake and two-photon live cell fluorescence imaging.[37] In this work, a tautomeric organic cage (**OC1**) that shows unprecedented photostability for live-cell imaging with high biocompatibility, cell permeability and mitochondrial targetability is reported (Fig. 1). We hypothesize that the keto–enol tautomerism is playing a major role in promoting the stability and sustaining the fluorescence of this platform. Such effect has been previously reported in other organic dyes such as oxyluciferin and HDFL.[38,39]

[a]*Smart Hybrid Materials (SHMs) Laboratory, Advanced Membranes and Porous Materials Center, King Abdullah University of Science and Technology (KAUST), Thuwal 23955-6900, Kingdom of Saudi Arabia. E-mail: niveen.khashab@kaust.edu.sa*

[b]*King Abdullah University of Science and Technology, Biological and Environmental Science and Engineering Division, Thuwal 23955-6900, Saudi Arabia*

† Electronic supplementary information (ESI) available. CCDC 2144153. For ESI and crystallographic data in CIF or other electronic format see https://doi.org/10.1039/d2sc00836j

‡ D. K and A. D contributed equally to this work.

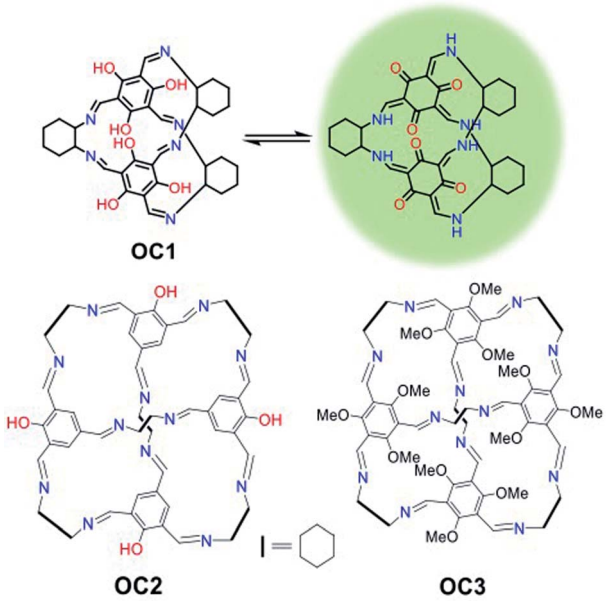

Fig. 1 Tautomeric forms of **OC1** and chemical structures of **OC2** and **OC3**.

Investigating other organic cages with less hydroxyl groups (**OC2**) or replacing the hydroxyl groups with methoxy substituents (**OC3**) resulted in the loss of cell stability, retention and targetability (Fig. 1). The presence of the –OH groups in **OC1** not only enables keto–enol tautomerization but also promotes H-bonding interactions, which ultimately improves solubility and cell permeability. We envision that understanding the nature of the intra- and intermolecular interactions in organic probes can lead to a profound enhancement in the photobleaching efficacy in addition to cell permeability. **OC1** can effectively image the mitochondria over 3 h with high selectivity and without any loss of efficacy (no photo bleaching), which is comparable to the commercially used MitoTracker RedFM.

OC1, a [2 + 3] cage, was synthesized following a reported procedure and its structure was confirmed by ^{1}H Nuclear Magnetic Resonance (NMR) and TOF-Mass analysis (Fig. S1–S4†).[32] Dynamic light scattering (DLS) of **OC1** revealed an average size of 30–50 nm in DMSO–H_2O (2–5%) with a negative zeta potential of −5 mV (Fig. S5†). Single crystal X-ray analysis revealed that **OC1** crystallizes in a triclinic crystal system with chiral *P*1 space group and the asymmetric unit consists of two molecules of [2 + 3] cages (Fig. S6†). Crystal structure analysis suggests that the imine cage crystallizes as the keto tautomeric form (Fig. 2a). This results in the formation of intramolecular N–H···O hydrogen bonding between the imine (N–H) hydrogen and the keto (C=O) oxygen ($d_{\text{C–OH actual}} = 1.36$ Å; $d_{\text{C=O actual}} =$ 1.25–1.26 Å *vs.* $d_{\text{C=O for OC1}} = 1.260$ Å and $d_{\text{C=N actual}} = 1.25$ Å *vs.* $d_{\text{C–NH for OC1}} = 1.30$–$1.35$ Å) (Fig. S6†). Three different windows of each cage are connected with three different cages in the same plane through weak C–H···O hydrogen bonding ($d = 2.414$ Å, and $\theta = 60°$), which creates isolated pores at the center of the cage (Fig. 2b). Furthermore, the packing diagram suggests the formation of one-dimensional infinite extrinsic pores along the *b*-axis (Fig. 2c and S6†). **OC1** is stable in aqueous solutions even at low pH as well as in cell media (Fig. S7–S10†).

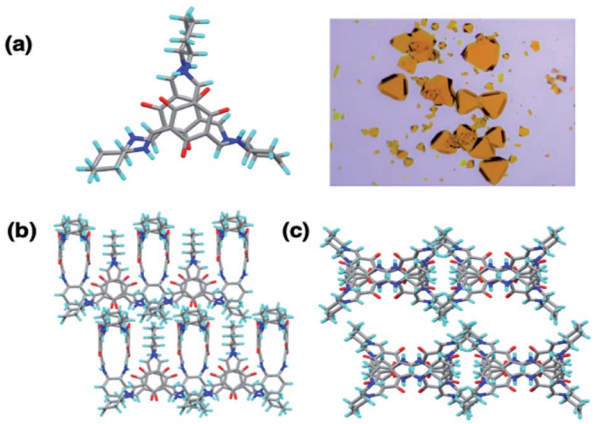

Fig. 2 (a) SCXRD and crystal image of **OC1**. (b) **OC1** self-assembled through hydrogen bonding interactions. (c) Packing of **OC1** along *b*-axis.

To test our original proposal that organic cages can act as effective imaging agents, we first investigated the UV-visible spectrum of **OC1** in DMSO, which exhibited two characteristic peaks at $\lambda_{max} = 286$ and 330 nm that can be assigned to π–π* and n–π* transitions, respectively (Fig. S11†). Fluorescence emission spectra showed that **OC1** exhibits two major peaks at around 411 and 497 nm upon excitation at 330–350 nm in DMSO, while excitation at 400 and 480 nm showed characteristic emission peaks at 503 and 538 nm, respectively (Fig. S12†). This behavior can be explained by the presence of two emissive forms due to the keto–enol tautomerization. The quantum yield (QY) of **OC1** in DMSO (0.25) and chloroform (0.4) was also tested. Molar extinction coefficient of **OC1** was estimated as 46 806 M^{-1} cm^{-1} in DMSO (Fig. S13–S14†). The quantum yield of **OC1** in DMSO are about half that of in chloroform that is significantly matched with the reported intracellular targeted macrocyclic nanohoop structure.[37] The fluorescent properties of **OC1** were maintained at different pH values (4, 7 and 10) (Fig. S15†). We hypothesize that this mode of assembly, as supported by SCXRD, promotes stability and prevents aggregation-induced quenching that is very common in small molecule dye fluorophores. The keto–enol tautomerism is boosting intra- and intermolecular hydrogen bonding interactions that can be contributing to the emissive characteristics of this system. In fact, the presence of the phenolic OH groups have been reported to have critical effects on the structural and spectroscopic properties of organic cages.[31,40]

We then proceeded to test **OC1** for cell imaging by first testing the cytotoxicity of **OC1** in MCF-7 cells (Fig. S16a†). The cells were treated with a solution of concentrations ranging from 3.9–500 μg ml^{-1} for 24 h. Cell death was measured using MTT assay demonstrating the excellent biocompatibility of **OC1** with an IC50 of > 500 μg ml^{-1}. MCF-7 cells were then either co-incubated with **OC1** and LysoTracker Red or MitoTracker RedFM, the cells are then fixed with 4% formaldehyde (w/v) and imaged on a confocal laser-scanning microscope (CLSM).

Interestingly, **OC1** showed strong colocalization in the mitochondria with a Pearson's correlation coefficient of 0.9751 (Fig. S16b and c†). Real time imaging of MCF-7 cells at different time intervals after co-internalization of **OC1** and MitoTracker showed a clear signal overlap on a subcellular level (Fig. 3 and MOV1), which ultimately supports that **OC1** can selectively target the mitochondria.

These encouraging results piqued our interest to investigate other organic cages in order to have a better understanding of the mechanistic factors in play. As the tautomeric activity is well reported to affect the photophysical properties of organic compounds, we compared **OC1** to an organic cage with less phenolic OHs (**OC2**) and an organic cage with only methoxy substituents (**OC3**). **OC2** and **OC3** were synthesized and characterized according to reported procedures (Fig. S17–S25†).[32,41] Absorbance, emission properties and stabilities of **OC2** and **OC3** in DMSO were also verified. **OC2** showed one major characteristic emission peak at around 547 nm upon excitation at 350 and 440 nm. The quantum yield (QY) of **OC2** in DMSO (6.7%) and chloroform (11.1%) was also tested (Fig. S13 and S14†). **OC3** showed emission at 494 and 537 nm upon excitation at 320 nm and 480 nm upon excitation at 420 nm (Fig. S26†). The quantum yield (QY) and molar extinction coefficient of OC3 in DMSO is negligible. Cytotoxicity and biocompatibility studies of **OC2** and **OC3** showed a relatively higher cytotoxicity compared to **OC1** (Fig. S27†). As to targetability and photostability, **OC2** and **OC3** showed less selectivity with colocalization in both mitochondria and lysosome where the fluorescent signal slowly disappeared, which implies the **OC2** and **OC3** are less stable than **OC1** (Fig. S28†). Moreover, FACS data revealed that **OC1** showed the highest uptake percentage in comparison to **OC2**, and **OC3** with an uptake percentage of 86.4%, 78%, and 69%, respectively (Fig. S29†). Based on this data, we can conclude that indeed the hydroxyl groups, and their prompted keto–enol tautomerism, are playing a major role in stabilizing the overall structure through hydrogen bonding while simultaneously improving photostability and targetability. As a control, we tested the aldehyde starting material, 1,3,5-triformylphloroglucinol, to verify that **OC1** is being uptaken as a whole and not as the aldehyde building block or a possible decomposition product. The experiment clearly demonstrates that 1,3,5-triformylphloroglucinol as a fluorophore had no selectivity towards the mitochondria and is initially distributed in the cytoplasm and finally localizes in the lysosomes for degradation (Fig. S30†).

As for the uptake mechanism, we initially hypothesized that **OC1** will be taken up by cells through endocytosis, which is the typical biological pathway of nanoparticles and nanoassemblies.[42,43] Surprisingly, we discovered that **OC1** can passively diffuse rather than being actively transported through the cell membrane. Passive transport is a type of membrane transport that does not require energy to move substances across cell membranes as it mainly relies on the second law of thermodynamics. We tested **OC1** uptake in the presence of different endocytic inhibitors including chlorpromazine (CPZ), filipin (FIL), and amiloride to inhibit clathrin-mediated, caveolae mediated, and macropinocytotic endocytosis pathways, respectively.[44] All cells were treated with the inhibitors for 30 min, followed by 3 h incubation with **OC1**. The cellular uptake data showed that there was no significant reduction in the uptake using the active transport inhibitors (Fig. 4a). Moreover, the passive transport was tested by incubating **OC1** (125 μg ml^{-1}) with MCF-7 for 3 h at different temperatures (4, 27, or 37 °C). The uptake was monitored by confocal microscopy (Fig. 4b) and quantified by FACS (Fig. 4c). Interestingly, no obvious reduction of uptake was observed in all the cases.

After verifying the targetability and the uptake mechanism of **OC1**, we focused our attention on photostability. Since the commercially available mitochondrion tracker dyes normally have moderate photostability, it is critical to evaluate the photostability of **OC1** in live cells. We first compared the photostability of **OC1** with the commercially available MitoTracker RedFM. Since the excitation/emission wavelengths of **OC1** (abs/em ~495/519 nm) and MitoTracker RedFM (abs/em ~581/644 nm) are distant from each other, we performed simultaneous scans for both dyes for 100 scans at 1.5 s per scan by incubating **OC1** and MitoTracker RedFM with MCF-7 cells at 37 °C for 48 h. The results showed that at a laser power density of $P \sim 0.4132$ W cm^{-2} **OC1** ($\varepsilon = 46\,806$ M^{-1} cm^{-1}) had higher retention and photostability than that of the MitoTracker RedFM where **OC1** retained 54% of its initial fluorescence intensity while the fluorescence of MitoTracker RedFM dropped below 15% (Fig. 5a). Moreover, **OC1** showed high photostability even at 72 h post-staining (Fig. 5b). Finally, it was noted that throughout the 72 h of incubation of **OC1** with MCF-7, over three generations occurred in the cell culture and showed fluorescent labeling of the mitochondria suggesting that **OC1** can be passed through to daughter cells upon cell division.

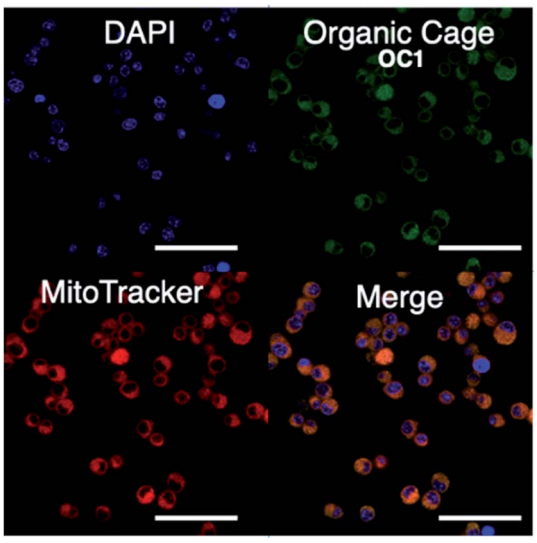

Fig. 3 Live cell imaging of MCF-7 cells incubated with 250 μg ml^{-1} of **OC1** for 3 h showing the uptake and colocalization of **OC1** (abs/em ~495/519 nm) with the commercial probe MitoTracker RedFM (abs/em ~581/644 nm) in the mitochondria (scale bar at 50 μm).

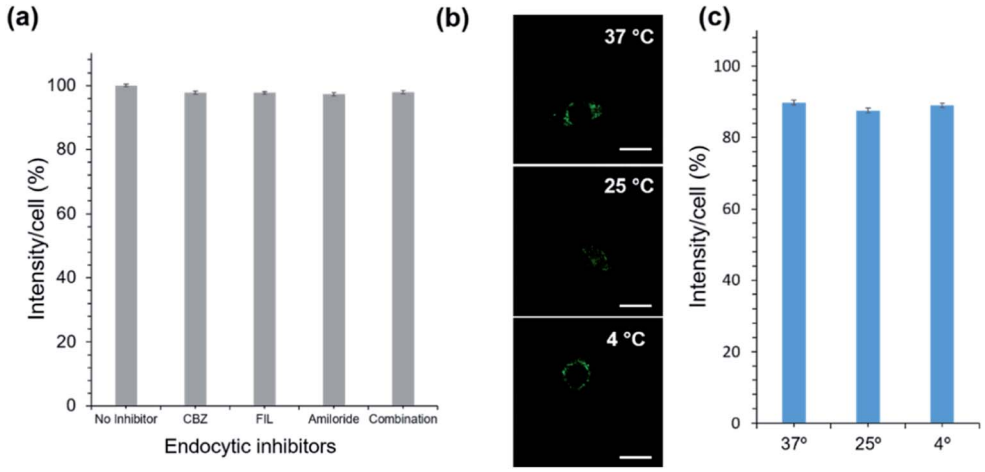

Fig. 4 Cellular uptake mechanism of **OC1**. (a) Cell uptake of **OC1** in the presence of endocytosis inhibitors to investigate endocytic uptake mechanism. (b) MCF-7 cell uptake CLSM of **OC1** at 37 °C, 25 °C, and 4 °C, respectively (scale bar at 30 μm). (c) Quantification of cell fluorescence relative to 37 °C.

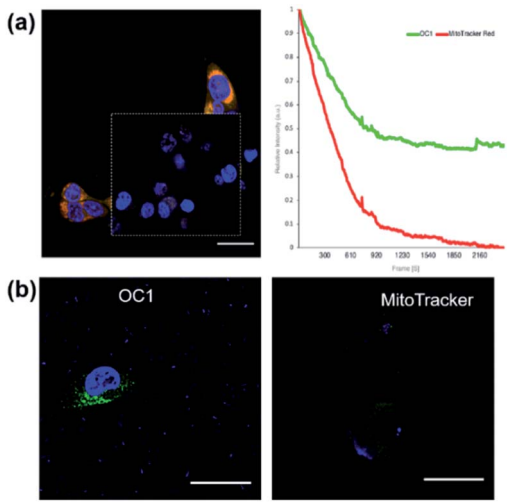

Fig. 5 Intracellular retention and photostability of **OC1**. (a) Photostability of **OC1** in MCF-7 cells co incubated with MitoTracker RedFM for 48 h. Plot of the sum intensity of each frame normalized to time 0 (frame 1) and plotted against time (seconds). Intensity data analysis was done using Python and plotted on Excel. (b) CLSM images (72 h post incubation) showing **OC1** distribution while most of the MitoTracker RedFM signal was lost (Scale bar at 30 μm).

Conclusions

In summary, we demonstrated that a biocompatible organic cage (**OC1**) can be efficiently employed as a mitochondria-targeted fluorescent probe with high cell permeability and impressive photostability. We investigated the role of the keto–enol tautomerism in improving the stability, fluorescence and cell retention of **OC1** where it outperformed the commercially used MitoTracker RedFM. This work demonstrates the relatively unexplored potential of organic cages for use in biomedical applications. Moreover, it highlights the importance of inter- and intramolecular interactions to stabilize and improve the performance of current fluorophores. Understanding the interactions and assemblies at a molecular level can provide a solid base for the rational design and synthesis of the next generation fluorescent tags with superior physiological profiles and exceptional photostability.

Data availability

Full experimental and crystallographic details are provided as part of the ESI. CCDC 2144153.†

Author contributions

DK: investigation, validation, data collection, formal analysis, writing original draft. AD: conceptualization, synthesis, validation, investigation, data collection, formal analysis, writing original draft, review & editing. LA: formal analysis. HP: formal analysis, data collection. SH: discussion. NMK: supervision the project, funding acquisition, writing, review & editing.

Conflicts of interest

There are no conflicts to declare.

Notes and references

1 J. Chan, S. C. Dodani and C. J. Chang, Reaction-based small-molecule fluorescent probes for chemoselective bioimaging, *Nat. Chem.*, 2012, **4**, 973.
2 S. Hapuarachchige, G. Montaño, C. Ramesh, D. Rodriguez, L. H. Henson, C. C. Williams, S. Kadavakkollu, D. L. Johnson, C. B. Shuster and J. B. Arterburn, Design and Synthesis of a New Class of Membrane-Permeable Triazaborolopyridinium Fluorescent Probes, *J. Am. Chem. Soc.*, 2011, **133**, 6780–6790.
3 A. N. Butkevich, G. Lukinavičius, E. D'Este and S. W. Hell, Cell-Permeant Large Stokes Shift Dyes for Transfection-

Free Multicolor Nanoscopy, *J. Am. Chem. Soc.*, 2017, **139**, 12378–12381.

4 C. J. MacNevin, T. Watanabe, M. Weitzman, A. Gulyani, S. Fuehrer, N. K. Pinkin, X. Tian, F. Liu, J. Jin and K. M. Hahn, Membrane-permeant, environment-sensitive dyes generate biosen-sors within living cells, *J. Am. Chem. Soc.*, 2019, **141**, 7275–7282.

5 A. F. L. Schneider, L. S. Benz, M. Lehmann and C. P. R. Hackenberger, Cell-Permeable Nanobodies Allow Dual-Color Super-Resolution Microscopy in Untransfected Living Cells, *Angew. Chem., Int. Ed.*, 2021, **60**, 22075–22080.

6 T. Myochin, K. Hanaoka, T. Komatsu, T. Terai and T. Nagano, Design Strategy for a Near-Infrared Fluorescence Probe for Matrix Metalloproteinase Utilizing Highly Cell Permeable Boron Dipyrro-methene, *J. Am. Chem. Soc.*, 2012, **134**, 13730–13737.

7 M. Grzybowski, M. Taki, K. Senda, Y. Sato, T. Ariyoshi, Y. Okada, R. Kawakami, T. Imamura and S. Yamaguchi, A Highly Photostable Near-Infrared Labeling Agent Based on a Phospha-rhodamine for Long-Term and Deep Imaging, *Angew. Chem., Int. Ed.*, 2018, **57**, 10137–10141.

8 V. Glembockyte, M. Frenette, C. Mottillo, A. M. Durantini, J. Gostick, V. Štrukil, T. Friščić and G. Cosa, Highly Photostable and Fluorescent Microporous Solids Prepared *via* Solid-State Entrap-ment of Boron Dipyrromethene Dyes in a Nascent Metal–Organic Framework, *J. Am. Chem. Soc.*, 2018, **140**, 16882–16887.

9 X. Wu and W. Zhu, Stability enhancement of fluorophores for lighting up practical application in bioimaging, *Chem. Soc. Rev.*, 2015, **44**, 4179–4184.

10 G. T. Nash, T. Luo, G. Lan, K. Ni, M. Kaufmann and W. Lin, Nanoscale Metal–Organic Layer Isolates Phthalocyanines for Effi-cient Mitochondria-Targeted Photodynamic Therapy, *J. Am. Chem. Soc.*, 2021, **143**, 2194–2199.

11 T. Luo, G. T. Nash, Z. Xu, X. Jiang, J. Liu and W. Lin, Nanoscale Metal–Organic Framework Confines Zinc-Phthalocyanine Photosensitizers for Enhanced Photodynamic Therapy, *J. Am. Chem. Soc.*, 2021, **143**, 13519–13524.

12 C. Grunwald, K. Schulze, G. Giannone, L. Cognet, B. Lounis, D. Choquet and R. Tampé, Quantum-Yield-Optimized Fluorophores for Site-Specific Labeling and Super-Resolution Imaging, *J. Am. Chem. Soc.*, 2011, **133**, 8090–8093.

13 R. Kimura, H. Kuramochi, P. Liu, T. Yamakado, A. Osuka, T. Tahara and S. Saito, Flapping Peryleneimide as a Fluorogenic Dye with High Photostability and Strong Visible-Light Absorption, *Angew. Chem., Int. Ed.*, 2020, **59**, 16430–16435.

14 K. Henze and W. Martin, Evolutionary biology: essence of mito-chondria, *Nature*, 2003, **426**, 127.

15 D. C. Wallace, Mitochondrial Diseases in Man and Mouse, *Science*, 1999, **283**, 1482–1488.

16 H. Zhu, J. Fan, J. Du and X. Peng, Fluorescent Probes for Sens-ing and Imaging within Specific Cellular Organelles, *Acc. Chem. Res.*, 2016, **49**, 2115–2126.

17 W. Xu, Z. Zeng, J.-H. Jiang, Y.-T. Chang and L. Yuan, Discerning the Chemistry in Individual Organelles with Small-Molecule Fluorescent Probes, *Angew. Chem., Int. Ed.*, 2016, **55**, 13658–13699.

18 S. Luo, X. Tan, S. Fang, Y. Wang, T. Liu, X. Wang, Y. Yuan, H. Sun, Q. Qi and C. Shi, Mitochondria-Targeted Small-Molecule Fluorophores for Dual Modal Cancer Phototherapy, *Adv. Funct. Mater.*, 2016, **26**, 2826–2835.

19 W.-C. Geng, Z. Ye, Z. Zheng, J. Gao, J. –J. Li, M. R. Shah, L. Xiao and D. –S. Guo, Supramolecular Bioimaging through Sig-nal Amplification by Combining Indicator Displacement Assay with Förster Resonance Energy Transfer, *Angew. Chem., Int. Ed.*, 2021, **60**, 19614–19619.

20 D. Pendin, R. Norante, A. D. Nadai, G. Gherardi, N. Vajente, E. Basso, N. Kaludercic, C. Mammucari, C. Paradisi, T. Pozzan and A. Mattarei, A Synthetic Fluorescent Mitochondria-Targeted Sensor for Ratiometric Imaging of Calcium in Live Cells, *Angew. Chem., Int. Ed.*, 2019, **58**, 9917–9922.

21 Y. Han, M. Li, F. Qiu, M. Zhang and Y.-H. Zhang, Cell-permeable organic fluorescent probes for live-cell long-term super-resolution imaging reveal lysosome-mitochondrion interactions, *Nat. Commun.*, 2017, **8**, 1307.

22 G. Hong, S. Diao, A. L. Antaris and H. Dai, Carbon Nanomaterials for Biological Imaging and Nanomedicinal Therapy, *Chem. Rev.*, 2015, **115**, 10816–10906.

23 R. K. Pathak, N. Kolishetti and S. Dhar, Targeted Nanoparticles in Mitochondrial Medicine, *Wiley Interdiscip. Rev.: Nanomed. Nanobiotechnol.*, 2015, **7**, 315–329.

24 H. Kobayashi, M. Ogawa, R. Alford, P. L. Choyke and Y. Urano, New Strategies for Fluorescent Probe Design in Medical Diagnostic Imaging, *Chem. Rev.*, 2010, **110**, 2620–2640.

25 H.-T. Feng, Y.-X. Yuan, J.-B. Xiong, Y.-S. Zheng and B. Z. Tang, Macrocycles and cages based on tetraphenylethylene with aggregation-induced emission effect, *Chem. Soc. Rev.*, 2018, **47**, 7452–7476.

26 Y. Kawazoe, H. Shimogawa, A. Sato and M. Uesugi, A Mitochondrial Surface-Specific Fluorescent Probe Activated by Biocon-version, *Angew. Chem.*, 2011, **123**, 5592–5595.

27 C. W. L. Leung, Y. Hong, S. Chen, E. Zhao, J. W. Y. Lam and B. Z. Tang, A Photostable AIE Luminogen for Specific Mitochon-drial Imaging and Tracking, *J. Am. Chem. Soc.*, 2013, **135**, 62–65.

28 T. Tozawa, J. T. A. Jones, S. I. Swamy, S. Jiang, D. J. Adams, S. Shakespeare, R. Clowes, D. Bradshaw, T. Hasell, S. Y. Chong, C. Tang, S. Thompson, J. Parker, A. Trewin, J. Bacsa, A. M. Z. Slawin, A. Steiner and A. I. Cooper, Porous organic cages, *Nat. Mater.*, 2009, **8**, 973–978.

29 J. R. Holst, A. Trewin and A. I. Cooper, Porous organic molecules, *Nat. Chem.*, 2010, **2**, 915.

30 T. Hasell and A. I. Cooper, Porous organic cages: soluble, modu-lar and molecular pores, *Nat. Rev. Mater.*, 2016, **1**, 16053.

31 M. Mastalerz, Porous Shape-Persistent Organic Cage Compounds of Different Size, Geometry, and Function, *Acc. Chem. Res.*, 2018, **51**, 2411–2422.

32 S. Bera, A. Basu, S. Tothadi, B. Garai, S. Banerjee, K. Vanka and R. Banerjee, Porosity Switching in Polymorphic Po-

rous Organic Cages with Exceptional Chemical Stability, *Angew. Chem.*, 2019, **131**, 4287–4291.

33 M. Mastalerz, M. W. Schneider, I. M. Oppel and O. Presly, A Salicylbisimine Cage Compound with High Surface Area and Selective CO_2/CH_4 Adsorption, *Angew. Chem., Int. Ed.*, 2011, **50**, 1046–1051.

34 B. Moosa, L. O. Alimi, A. Shkurenko, A. Fakim, P. M. Bhatt, G. Zhang, M. Eddaoudi and N. M. Khashab, A Polymorphic Azo-benzene Cage for Energy-Efficient and Highly Selective *p*-Xylene Separation, *Angew. Chem., Int. Ed.*, 2020, **59**, 21367–21371.

35 A. Dey, S. Chand, B. Maity, P. M. Bhatt, M. Ghosh, L. Cavallo, M. Eddaoudi and N. M. Khashab, Adsorptive Molecular Sieving of Styrene over Ethylbenzene by Trianglimine Crystals, *J. Am. Chem. Soc.*, 2021, **143**, 4090–4094.

36 X. Zheng, W. Zhu, C. Zhang, Y. Zhang, C. Zhong, H. Li, G. Xie, X. Wang and C. Yang, Self-Assembly of a Highly Emissive Pure Organic Imine-Based Stack for Electroluminescence and Cell Imag-ing, *J. Am. Chem. Soc.*, 2019, **141**, 4704–4710.

37 T. C. Lovell, S. G. Bolton, J. P. Kenison, J. Shangguan, C. E. Otteson, F. Civitci, X. Nan, M. D. Pluth and R. Jasti, Subcellular Targeted Nanohoop for One- and Two-Photon Live Cell Imaging, *ACS Nano*, 2021, **15**(9), 15285–15293.

38 Y. Cheng, G. Li, Y. Liu, Y. Shi, G. Gao, D. Wu, J. Lan and J. You, Unparalleled Ease of Access to a Library of Biheteroaryl Fluorophores *via* Oxidative Cross-Coupling Reactions: Discovery of Photostable NIR Probe for Mitochondria, *J. Am. Chem. Soc.*, 2016, **138**(14), 4730–4738.

39 T.-B. Ren, Q.-L. Zhang, D. Su, X.-X. Zhang, L. Yuan and X. – B. Zhang, Detection of analytes in mitochondria without inter-ference from other sites based on an innovative ratiometric fluoro-phore, *Chem. Sci.*, 2018, **9**, 5461–5466.

40 P. Kieryk, J. Janczak, J. Panek, M. Miklitz and J. Lisowski, Chiral 2 + 3 Keto-Enamine Pseudocyclophanes Derived from 1,3,5-Triformylphloroglucinol, *Org. Lett.*, 2016, **18**, 12–15.

41 M. Petryk, J. Szymkowiak, B. Gierczyk, G. Spólnik, Ł. Popenda, A. Janiak and M. Kwit, Chiral, triformylphenol-derived salen-type [4 + 6] organic cages, *Org. Biomol. Chem.*, 2016, **14**, 7495–7499.

42 J. Wagner, L. Li, J. Simon, K. Landfester, V. Mailänder, K. Müllen, D. Y. W. Ng, Y. Wu, T. Weil and L. Krutzke, Amphiphilic Polyphenylene Dendron Conjugates for Surface Remodeling of Adenovirus, *Angew. Chem., Int. Ed.*, 2020, **59**, 5712.

43 R. Stangenberg, Y. Wu, J. Hedrich, D. Kurzbach, D. Wehner, G. Weidinger, S. L. Kuan, M. I. Jansen, F. Jelezko, H. J. Luhmann, D. Hinderberger, T. Weil and K. Müllen, A Polyphenylene Den-drimer Drug Transporter with Precisely Positioned Amphiphilic Surface Patches, *Adv. Healthcare Mater.*, 2015, **4**, 377–384.

44 N. J. Yang and M. J. Hinner, Getting across the Cell Membrane: An Overview for Small Molecules, Peptides, and Proteins, *Methods Mol. Biol*, 2015, **1266**, 29–53.